European Journal of Mechanics / B Fluids 87 (2021) 151–160

Contents lists available at ScienceDirect

European Journal of Mechanics / B Fluids

journal homepage: www.elsevier.com/locate/ejmflu

The Green function for diffraction and radiation of regular waves by two-dimensional structures

Ed Mackay

College of Engineering, Mathematics and Physical Sciences, University of, Exeter, TR10 9FE, UK

ARTICLE INFO

Article history:
Received 12 October 2020
Received in revised form 29 January 2021
Accepted 30 January 2021
Available online 9 February 2021

Keywords:
Green function
Boundary element method
Asymptotic analysis
Added mass
Damping

ABSTRACT

New expressions are derived for the Green function (GF) for diffraction and radiation of waves by a two-dimensional (2D) body in finite water depth. The finite depth GF is expressed as a sum of singularities, the infinite depth GF and smoothly-varying integrals that are convergent for all parameter values. The infinite depth component is given explicitly, making it very fast to compute. Explicit expressions are derived for the limiting cases of zero and infinite frequency, for both finite and infinite water depth. The low frequency limit of the 2D GF is inconsistent with the zero-frequency 2D GF, with the real part tending to infinity when the water depth is infinite and the imaginary part tending to infinity in finite water depth. The inconsistencies with the zero frequency GF differ between the 2D and 3D cases. These inconsistencies lead to differences between the low-frequency behaviour of the added mass and damping of an oscillating body and the values at zero frequency. It is shown that these differences can be inferred directly from the behaviour of the GF at low frequencies.

1. Introduction

The boundary element method (BEM) is often used to solve wave–structure interaction problems in two and three dimensions. Two-dimensional (2D) problems arise as idealisations of sections of three-dimensional (3D) flows. Examples of 2D problems include tests in narrow flumes or the strip theory for ship motions [1–3]. BEM models use Green's theorem together with a suitable Green function (GF) to formulate an integral equation for the velocity potential over the surface of a body (or bodies) [4,5]. In 3D BEM models it is common to use a GF that satisfies the free-surface and sea bed boundary conditions as well as the Laplace equation and a radiation condition in the far field. This reduces the domain of the resulting integral equations, to cover only the structure(s) of interest. In 2D BEM models, many practitioners opt to use a simpler GF, corresponding to the fundamental solution of the Laplace equation (e.g. [6–11]). This has the advantage that calculation of the GF is very fast, but at the cost of having to expand the domain of the integral equations to cover the free surface, sea bed and a control surface in the far field, as well as the structure of interest. Compared to 3D BEM models, this is a relatively low cost, since the number of panels required to cover these surfaces is much lower in 2D than in 3D.

For certain problems an iterative solution to the BEM equations is required. For example, for wave interaction with porous structures, the pressure-drop across the porous surface is proportional to the square of the velocity [12]. This results in a set of integral equations, in which the coefficients contain unknowns that must be determined iteratively [9–11,13,14]. For these problems it can be advantageous to use a GF which satisfies the free-surface, sea bed and radiation boundary conditions to reduce the domain of the integral equations and hence the size of the linear system which must be solved iteratively.

Calculation of the free-surface GF in 3D has received a lot of attention in the literature over the years [15–27]. Approaches proposed include polynomial approximation [28–30], eigenfunction expansion [31], representation in terms of ordinary differential equations [32–34] or approximation in terms of standard functions [35]. In comparison, the calculation of the 2D free-surface GF has received less attention. John [16] derived series and integral expressions for the GF in 2D and 3D. A general procedure for the construction of 2D and 3D free-surface GF's for Laplace's equation was presented by Thorne [36]. Wehausen and Laitone [37] reviewed various formulations for the 2D GF. More recent reviews were provided by Mei [38] and Linton and McIver [4]. Hein et al. [39] showed that in infinite depth, the local flow component of the 2D GF can be expressed in terms of the exponential integral, allowing fast calculation using standard algorithms.

In finite water depth, the series expansion of the 2D GF given by John [16] converges rapidly when the horizontal distance between the source and field points is sufficiently large. In the near-field, the series is slow to converge, making the integral representation more attractive for computations. However, the integral representation given by John [16] is divergent when both the source and field point are located on the free surface. A similar

E-mail address: e.mackay@exeter.ac.uk.

https://doi.org/10.1016/j.euromechflu.2021.01.012

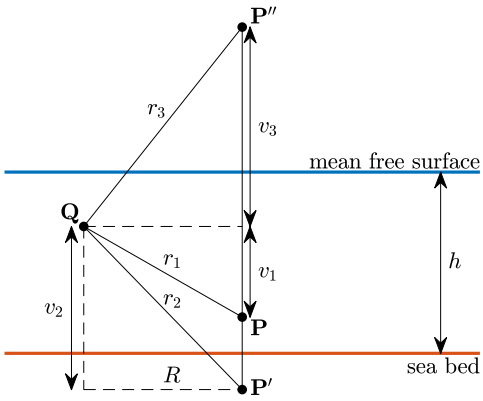

Fig. 1. Sketch of variables used in the definition of the Green function.

issue occurs for integral representation of the finite depth GF in 3D. Newman [22] showed that the integral for the 3D finite depth GF could be made to converge by subtracting the infinite depth component. A similar approach was used in subsequent studies to derive various integrals which can be approximated by Chebyshev polynomials [28–30]. The same approach can be applied to the 2D finite depth GF. In this work, we follow a similar approach to Mackay [30] to obtain integral expressions for the 2D GF which are convergent for all parameter values. The integral expressions derived here also have the advantage that they are slowly-varying in the parameters, making them readily-amenable to numerical approximation. We also consider the limiting behaviour of the 2D GF in infinite water depth, in the far field and for the cases of zero and infinite frequency.

An unusual feature of the GF in both 2D and 3D is that the limiting behaviour for low frequencies is inconsistent with the zero-frequency GF, with some components tending to infinity as the frequency tends to zero. The zero and infinite frequency limits of the 3D GF have been considered by various authors [16,22,28, 30,40,41]. In this work we consider the low frequency behaviour of the 2D GF and show that inconsistencies with the zero frequency GF differ between the 2D and 3D cases and the finite and infinite depth cases.

These inconsistencies lead to differences between the low-frequency behaviour of the added mass and damping of an oscillating body and the values at zero frequency. This peculiar behaviour of the added mass and damping for low frequencies have been known for a long time. Ursell [42] considered the case of a heaving half-immersed circular 2D cylinder and noted that the added mass tends to infinity in finite depth, but tends to a finite limit for deep water. The general case of added mass and damping of a heaving symmetric body in two dimensions was considered by McIver and Linton [43], who noted that for finite water depth the non-dimensional damping tends to infinity as the frequency tends to zero. Kotik and Mangulis [44] used the Kramers–Kronig relations to show that for a floating 3D hemisphere in finite depth the heave added mass tends to infinity and the non-dimensionalised damping tends to a finite limit. This limiting behaviour of either infinite added mass or infinite damping is not physically realistic. Chen et al. [41] noted that the inconsistency between the non-physical behaviour is related to the assumption of an incompressible fluid. They report that when compressibility is accounted for, the wavenumber tends to a non-zero value at zero frequency and the singularity associated with zero wavenumber disappears, however the analysis is referred to an unpublished report. In this work we present a brief comparison of the 2D and 3D GFs and discuss their limiting behaviour at low frequency. It is shown that the limiting behaviour of the added mass and damping can be inferred directly from the behaviour of the GF at low frequencies.

The paper is organised as follows. The boundary value problem that the 2D GF satisfies is defined in Section 2. John's series expansion is presented in Section 3 and the convergence properties are considered. New integral expressions for the 2D GF are derived in Section 4. The far-field limit is considered in Section 5 and the cases of zero and infinite frequency are considered in Sections 6 and 7. A brief comparison of the 2D and 3D GFs is presented in Section 8. The effect of the low frequency behaviour of the GF on added mass and damping is discussed in Section 9. Finally, a discussion and conclusions are presented in Section 10. For readers wishing to implement the expressions derived in this work, a summary of the relevant equations is presented in Table 2.

2. Formulation and notation

Consider a pulsating source located at $\mathbf{P} = (\xi, \zeta)$ in water of depth h, oscillating at angular frequency ω. The Green function, $G(\mathbf{P}, \mathbf{Q})$, describes the spatial component of a velocity potential at field point $\mathbf{Q} = (x, z)$ of the form $\Phi(x, z, t) = \mathrm{Re}(G(\mathbf{P}, \mathbf{Q})e^{-i\omega t})$. A two-dimensional Cartesian coordinate system is defined with $z = 0$ on the mean free surface and $z = -h$ on the sea bed. The Green function satisfies the Laplace equation in the fluid domain, the linearised free-surface and seabed boundary conditions, and a radiation condition in the far field, given by

$$\nabla^2 G = \frac{1}{2\pi}\delta(x-\xi)\delta(z-\zeta), \qquad \text{in the fluid} \tag{1a}$$

$$\frac{\partial G}{\partial z} = KG, \qquad z = 0, \tag{1b}$$

$$\frac{\partial G}{\partial z} = 0, \qquad z = -h, \tag{1c}$$

$$\frac{\partial G}{\partial x} = \pm ik_0 G, \qquad k_0(x-\xi) \to \pm\infty, \tag{1d}$$

where $\delta(\cdot)$ is the Dirac delta function, $K = \omega^2/g$ and g is the acceleration due to gravity. k_0 is the wavenumber, defined as the positive real solution of the dispersion equation

$$K = k\tanh(kh). \tag{2}$$

It is useful to define the variables

$$v_1 = |z-\zeta|, \;\; v_2 = 2h - v_3, \;\; v_3 = |z+\zeta|, \;\; v_4 = 2h - v_1 \tag{3a}$$

$$R = |x-\xi|, \;\; r_j = \left(R^2 + v_j^2\right)^{1/2}, \tag{3b}$$

and nondimensional variables

$$H = Kh, \;\; A = R/h, \;\; B_j = v_j/h, \tag{4a}$$

$$X = KR, \;\; V_j = K v_j. \tag{4b}$$

A sketch of the distances corresponding to the dimensional variables is shown in Fig. 1. The variable r_1 is the distance from $\mathbf{P}$ to $\mathbf{Q}$, r_2 is the distance from the $\mathbf{Q}$ to $\mathbf{P}'$, the image of $\mathbf{P}$ in the sea bed and r_3 is the distance from $\mathbf{Q}$ to $\mathbf{P}''$, the image of $\mathbf{P}$ in the free surface. For the nondimensional variables, note that $B_1 \in [0, 1]$, $B_2 \in [0, 2]$, $B_3 = 2 - B_2 \in [0, 2]$ and $B_4 = 2 - B_1 \in [1, 2]$.

3. Series expressions

3.1. Finite depth

John [16] showed that the 2D GF in finite water depth can be expressed as:

$$\begin{aligned} G = &-2\pi i C_0 \cosh(k_0(z+h))\cosh(k_0(\zeta+h))\exp(ik_0 R) \\ &- 2\pi \sum_{n=1}^{\infty} C_n \cos(k_n(z+h))\cos(k_n(\zeta+h))\exp(-k_n R), \end{aligned} \tag{5}$$

where

$$C_0 = \frac{1}{k_0}\frac{k_0^2 - K^2}{(k_0^2 - K^2)h + K}, \tag{6a}$$

$$C_n = \frac{1}{k_n}\frac{k_n^2 + K^2}{(k_0^2 + K^2)h + K}, \tag{6b}$$

and k_n are the positive real roots of $K = -k\tan(kh)$, ordered in increasing value. The terms involving k_0 represent the propagating wave, while the series represents the local disturbance, which decreases exponentially away from the source.

The expression above is not the most convenient for numerical calculations at higher values of Kh, since C_0 decreases exponentially with Kh, whilst the hyperbolic terms increase exponentially with Kh. To avoid numerical inaccuracies, (5) can be rewritten using the relation

$$k_0^2 - K^2 = \frac{k_0^2}{\cosh^2(k_0 h)}, \tag{7}$$

which can be derived from the dispersion relation (2). Substituting this into (5) gives

$$\begin{aligned} G = &-2\pi i C_0' \frac{\cosh(k_0(z+h))}{\cosh(k_0 h)}\frac{\cosh(k_0(\zeta+h))}{\cosh(k_0 h)}\exp(ik_0 R) \\ &- 2\pi\sum_{n=1}^{\infty} C_n \cos(k_n(z+h))\cos(k_n(\zeta+h))\exp(-k_n R), \end{aligned} \tag{8}$$

where

$$C_0' = \frac{k_0}{(k_0^2 - K^2)h + K}. \tag{9}$$

In this form, $C_0' \to 1$ as $Kh \to \infty$ and the hyperbolic terms tend to $\exp(K(z+\zeta))$, which improves the accuracy of numerical computations.

The complex wavenumbers satisfy the inequality $(n - \frac{1}{2})\pi \leq k_n h \leq n\pi$, so for large n, $C_n \approx 1/n\pi$ and $\exp(-k_n R) \approx \exp(-n\pi R/h)$. This means that for small values of R/h the series is slow to converge. However, for $R/h \geq 0.5$, the error from truncating the series after the first 6 terms is less than 10^{-6}.

3.2. Infinite depth

As $h \to \infty$, the limit of the terms outside the series in (8) is $-2\pi i\exp(iX - V_3)$. However, $k_n \to (n - \frac{1}{2})\pi/h$ as $h \to \infty$, so we cannot substitute this directly into the series to obtain an expression for the series in infinite depth. Instead, an explicit expression for the infinite depth GF is derived from the integral expression in Section 4.2.

4. Integral expressions

4.1. Finite depth

For smaller values of R/h the GF can be written as an integral [16]

$$G = \log\left(\frac{r_1}{h}\right) + \log\left(\frac{r_2}{h}\right) - I, \tag{10}$$

where

$$\begin{aligned} \mathrm{Re}(I) = 2\cdot\mathrm{PV}\int_0^{\infty}\Bigg\{&(K+k)\frac{\cosh(k(z+h))\cosh(k(\zeta+h))}{k\sinh(kh) - K\cosh(kh)} \\ &\times\cos(kR) + 1\Bigg\}\frac{e^{-kh}}{k}dk, \end{aligned} \tag{11}$$

and $\mathrm{Im}(I)$ is given explicitly as the imaginary component of (5). The integrand of (11) has two real poles at $\pm k_0$ and infinitely many purely imaginary poles at $\pm ik_n$. Expanding the hyperbolic terms as exponentials and making the substitution $u = kh$ we can write

$$\mathrm{Re}(I) = L_1(A, B_1, H) + L_1(A, B_2, H), \tag{12}$$

where

$$\begin{aligned} L_1(A,B,H) = \mathrm{PV}\int_0^{\infty}\Big[&f(u,H)\left(e^{-u(2+B)} + e^{-u(2-B)}\right) \\ &\times\cos(uA) + e^{-u}\Big]\frac{du}{u} \end{aligned} \tag{13}$$

and

$$f(u,H) = \frac{u+H}{(u-H) - (u+H)e^{-2u}}. \tag{14}$$

The integral L_1 converges and is smoothly-varying for $B \leq 1$, but exhibits oscillatory behaviour for larger values of B and is divergent when $B = 2$. The values of L_1 for $A = 0$ and $A = 0.5$ are shown as a function of H for various values of B in Figs. 2 and 3. The integrals have been calculated using contour integration to avoid numerical issues close to the poles, using adaptive quadrature [45]. The poles of $f(u,H)$ are at $u = k_n h$. For small values of H we have $k_0 h \to \sqrt{H}$ and for large H we have $k_0 h \to H$. In particular we have $k_0 h \in [H, H + 0.3]$ for all H and $k_n h \in [n\pi - \frac{1}{2}, n\pi]$ for $n \geq 1$. We are therefore free to define any contour of integration that avoids these poles. For the present work, the path of integration is defined (arbitrarily) as the line connecting the points $\{0, H + i, H + 1, \infty\}$, illustrated in Fig. 4.

To force the integral to converge when $B = 2$, we can subtract the asymptotic form of $f(u,H)$ for large u. Define

$$g(u,H) = \left(f(u,H) - \frac{u+H}{u-H}\right)e^{2u} = \frac{(u+H)^2}{(u-H)^2 - (u^2 - H^2)e^{-2u}}. \tag{15}$$

Then we can write

$$\begin{aligned} L_1(A,B_2,H) = L_2(A,B_2,H) &+ \mathrm{PV}\int_0^{\infty}(e^{-u} - e^{-u/H})\frac{du}{u} \\ &+\mathrm{PV}\int_0^{\infty}\left[\frac{u+H}{u-H}e^{-uB_3}\cos(uA) + e^{-u/H}\right]\frac{du}{u}, \end{aligned} \tag{16}$$

where

$$\begin{aligned} L_2(A,B,H) = \mathrm{PV}\int_0^{\infty}\Big[&f(u,H)e^{-u(2+B)} + g(u,H)e^{-u(4-B)}\Big] \\ &\times\cos(uA)\frac{du}{u}. \end{aligned} \tag{17}$$

Using the identities [46, §3.476, §3.943]

$$\int_0^{\infty} e^{-bx}[1 - \cos(ax)]\frac{dx}{x} = \log\left(\frac{(a^2+b^2)^{1/2}}{b}\right), \tag{18}$$

$$\int_0^{\infty}(e^{-bu} - e^{-au})\frac{du}{u} = \log\left(\frac{a}{b}\right), \tag{19}$$

the second integral in (16) can be evaluated as

$$\int_0^{\infty}(e^{-u} - e^{-u/H})\frac{du}{u} = -\log(H), \tag{20}$$

and the third integral in (16) can be re-written as

$$\begin{aligned} &\mathrm{PV}\int_0^{\infty}\left[\frac{u+H}{u-H}e^{-uB_3}\cos(uA) + e^{-u/H}\right]\frac{du}{u} \\ &= 2\cdot\mathrm{PV}\int_0^{\infty}\frac{e^{-kV_3}\cos(kX)}{k-1}dk + \log\left((X^2 + V_3^2)^{1/2}\right). \end{aligned} \tag{21}$$

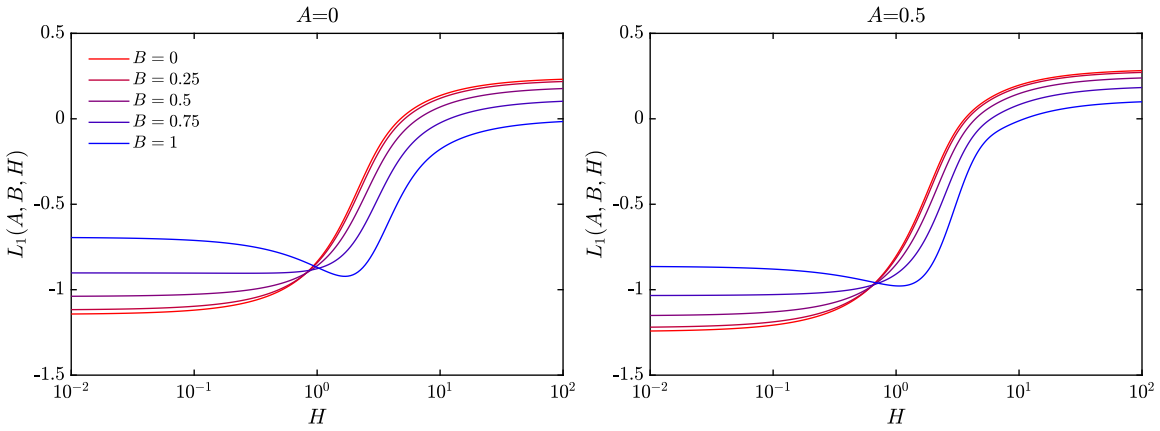

Fig. 2. The integral L_1 against H for $A = 0$ and $A = 0.5$ for various value of $B \in [0, 1]$.

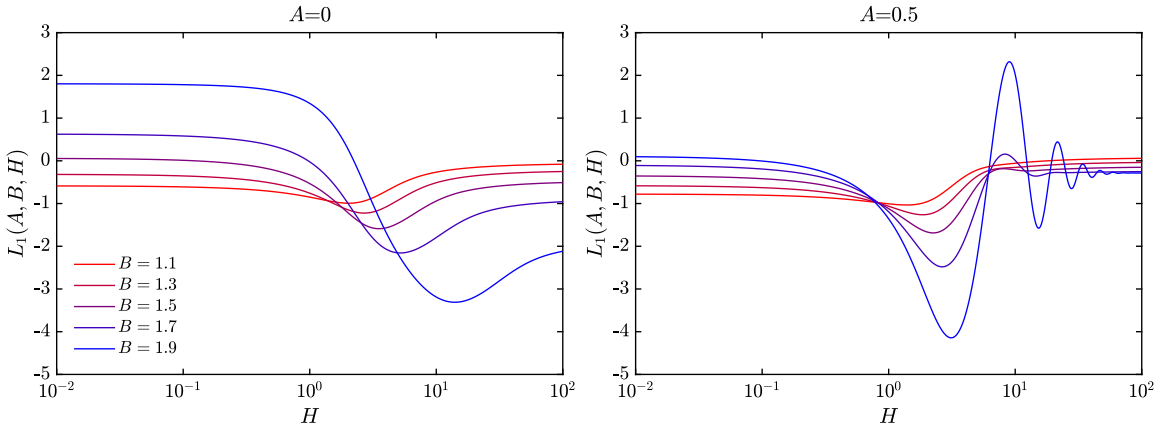

Fig. 3. The integral L_1 against H for $A = 0$ and $A = 0.5$ for various value of $B \in [1.1, 1.9]$.

Using the notation $Z = V_3 - iX$, the integral above can be expressed as

$$\begin{aligned}\mathrm{PV}\int_0^\infty \frac{e^{-kV_3}\cos(kX)}{k-1}dk &= \mathrm{Re}\left[\mathrm{PV}\int_0^\infty \frac{e^{-kZ}}{k-1}dk\right]\\ &= \mathrm{Re}\left[e^{-Z}(E_1(-Z)+i\pi)\right]\\ &= \mathrm{Re}\left[e^{-Z}E_1(-Z)\right]-\pi e^{-V_3}\sin(X),\end{aligned} \tag{22}$$

where E_1 is the exponential integral, defined as [47, §5.1]

$$E_1(z) = \int_z^\infty \frac{e^{-t}}{t}dt. \tag{23}$$

For $|Z| \to 0$ we have

$$\mathrm{Re}\left[e^{-Z}(E_1(-Z))\right] \to -\gamma - \log(|Z|), \tag{24}$$

where $\gamma \approx 0.57721$ is Euler's constant. It is convenient to define two functions

$$F_0(Z) = F_1(Z) + 2\log(|Z|), \tag{25a}$$

$$F_1(Z) = 2\mathrm{Re}\left[e^{-Z}E_1(-Z)\right] - 2\pi e^{-V_3}\sin(X), \tag{25b}$$

where $F_0(Z)$ is bounded for $|Z| \to 0$ and $F_1(Z)$ is bounded for X, V_3 away from zero. Substituting these expressions back into (16) gives

$$L_1(A, B_2, H) = L_2(A, B_2, H) - 2\log(H) + F_0(Z) - \log\left(\frac{r_3}{h}\right) \tag{26a}$$

$$= L_2(A, B_2, H) + F_1(Z) + \log\left(\frac{r_3}{h}\right) \tag{26b}$$

Recombining the expressions above, we can write the finite depth GF as

$$\begin{aligned}\mathrm{Re}(G) &= \log\left(\frac{r_1}{h}\right) + \log\left(\frac{r_2}{h}\right) + \log\left(\frac{r_3}{h}\right) - F_0(Z)\\ &\quad - L_1(A, B_1, H) - L_2(A, B_2, H) + 2\log(H) \qquad (27a)\\ &= \log\left(\frac{r_1}{h}\right) + \log\left(\frac{r_2}{h}\right) - \log\left(\frac{r_3}{h}\right) - F_1(Z)\\ &\quad - L_1(A, B_1, H) - L_2(A, B_2, H) \qquad (27b)\end{aligned}$$

For the calculation of L_2 we note that the function $g(u, H)$ has the same poles as $f(u, H)$ and an additional pole at $u = H$. We can therefore use the same contour of integration used for L_1, shown in Fig. 4. The values of L_2 are shown in Fig. 5 as a function of H for $A = 0$ and $A = 0.5$ and various values of $B \in [1, 2]$. The function $L_2(A, B, H) - 2\log(H)$ is bounded for $H \to 0$ and is smoothly varying in A, B and H. Similarly, $L_2(A, B, H)$ is bounded for $H \to \infty$ and smoothly-varying in the parameters. The integrals L_1 and L_2 are therefore both readily amenable to numerical approximation. Various authors have used Chebyshev polynomials for approximating the 3D Green function [28–30] and the same approach could be applied here as well. It will be shown in the next section that the function F_1 represents the local flow component and real part of the propagating wave for the infinite depth GF. There are many libraries of functions for calculating E_1 using continued fraction or series approximations [47, §5.1], making F_1 very fast to compute.

In the near-field, where $R/h \leq 0.5$, the expression (27a) is more appropriate for numerical calculations since F_0, L_1 and $L_2 - 2\log(H)$ are bounded and the remaining logarithmic terms

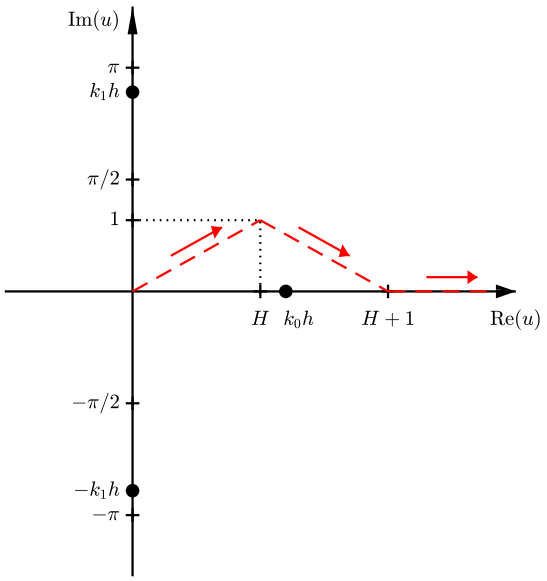

Fig. 4. Path of integration used for integrals L_1 and L_2.

can be integrated explicitly. In the region $R/h > 0.5$, the series (8) is rapidly-convergent and non-singular for all parameter values, so can be used instead.

4.2. Infinite depth

To derive an expression for infinite depth from (27a), we first consider the behaviour of the integrals L_1 and L_2. As $h \to \infty$ we have $H \to \infty$, $A, B_1 \to 0$ and $B_2 \to 2$. The limits of the functions f and g are therefore

$$\lim_{H\to\infty} f(u,H) = -\frac{1}{1+e^{-2u}}, \tag{28a}$$

$$\lim_{H\to\infty} g(u,H) = \frac{1}{1+e^{-2u}}. \tag{28b}$$

Substituting this into (13) and (17) gives

$$\lim_{H\to\infty} L_1(A,B_1,H) = \int_0^\infty \left[e^{-u} - \frac{2e^{-2u}}{1+e^{-2u}}\right]\frac{du}{u} = \log(4/\pi), \tag{29a}$$

$$\lim_{H\to\infty} L_2(A,B_2,H) = \int_0^\infty \left[\frac{e^{-2u}-e^{-4u}}{1+e^{-2u}}\right]\frac{du}{u} = \log(\pi/2). \tag{29b}$$

Finally, note that $r_2/h \to 2$ as $h \to \infty$. So combining this with the remaining terms in (27a) and taking the limit of the imaginary components in (8) gives

$$G^{deep} \overset{\text{def}}{=} \lim_{h\to\infty} G = \log(Kr_1) + \log(Kr_3) - 2\left(\mathrm{Re}\left[e^{-Z}E_1(-Z)\right] + \log(|Z|)\right) - 2\pi i e^{-Z}. \tag{30}$$

Here, the term $2\pi i e^{-Z}$ is the propagating wave, while the remaining terms represent a non-oscillatory local disturbance. A similar expression was derived by Hein et al. [39], but involving two exponential integrals rather than one. In the near-field, (30) is useful for numerical calculations, since the logarithmic singularities for $r_1 \to 0$ and $r_3 \to 0$ can be integrated explicitly, with the remaining terms being non-singular. For larger values of R, we can rewrite (30) as

$$G^{deep} = \log\left(\frac{r_1}{r_3}\right) - 2\mathrm{Re}\left[e^{-Z}E_1(-Z)\right] - 2\pi i e^{-Z}. \tag{31}$$

In this form, the terms $\log(r_1/r_3)$ and $\mathrm{Re}\left[e^{-Z}E_1(-Z)\right]$ are finite for $KR > 0$ and tend to zero for $R \to \infty$. The delineation for when to use each expression is somewhat arbitrary, but a reasonable choice would be to use the near-field form when $KR \leq 1$.

5. Far-field limit

The far-field form of the 2D GF is well known, but is included here for completeness. In the case of finite depth we start from (8) and note that as $R \to \infty$ the terms in the series decay to zero so

$$\lim_{R\to\infty} G = -2\pi i \frac{k_0}{(k_0^2-K^2)h+K}\frac{\cosh(k_0(z+h))}{\cosh(k_0h)} \times \frac{\cosh(k_0(\zeta+h))}{\cosh(k_0h)}\exp(ik_0R). \tag{32}$$

Then taking the limit for infinite depth we have

$$\lim_{R,\,h\to\infty} G = -2\pi i e^{-Z}. \tag{33}$$

6. Zero frequency limit

In the limit $K \to 0$ the free surface boundary condition (1b) tends to a homogeneous Neumann condition

$$\frac{\partial G}{\partial z} = 0, \quad z = 0. \tag{34}$$

In this case, G is only specified up to an arbitrary constant of integration. We consider the two cases of finite depth and infinite depth in turn below.

6.1. Finite depth

For the finite depth case, the series (8) can be used to obtain an explicit expression for the zero-frequency GF. The limits for the wavenumbers as $K \to 0$ are

$$k_0^2 \to K/h, \tag{35a}$$

$$k_n \to n\pi/h, . \tag{35b}$$

Using these, we obtain the following limits for the coefficients C_0' and C_n:

$$C_0' \to \frac{1}{2k_0h}, \tag{36a}$$

$$C_n \to \frac{1}{n\pi}. \tag{36b}$$

For the other terms involving k_0 we have the following limits as $K \to 0$

$$\frac{\cosh(k_0(z+h))}{\cosh(k_0h)}\frac{\cosh(k_0(\zeta+h))}{\cosh(k_0h)} \to 1, \tag{37a}$$

$$-2\pi i\exp(ik_0R) \to 2\pi(k_0R - i). \tag{37b}$$

Therefore, the real part of the first term of (8) tends to $\pi R/h$ and the imaginary part tends to an infinite limit that is independent of the spatial coordinates and can be disregarded in the definition of a zero-frequency GF. Substituting the expressions above into (8) we can define a zero-frequency GF as

$$\begin{aligned} G_0 &\overset{\text{def}}{=} \lim_{K\to 0}\left(G + \frac{i\pi}{k_0h}\right) \\ &= \pi A - 2\sum_{n=1}^{\infty}\frac{1}{n}\cos(n\pi z/h)\cos(n\pi\zeta/h)\exp(-n\pi A) \\ &= \pi A - \mathrm{Re}\left[\sum_{n=1}^{\infty}\frac{\exp(-n\pi(A+iB_1))}{n} + \sum_{n=1}^{\infty}\frac{\exp(-n\pi(A+iB_3))}{n}\right] \\ &= \pi A + \log\left(|1-\exp\left(-\pi(A+iB_1)\right)|\right) \end{aligned}$$

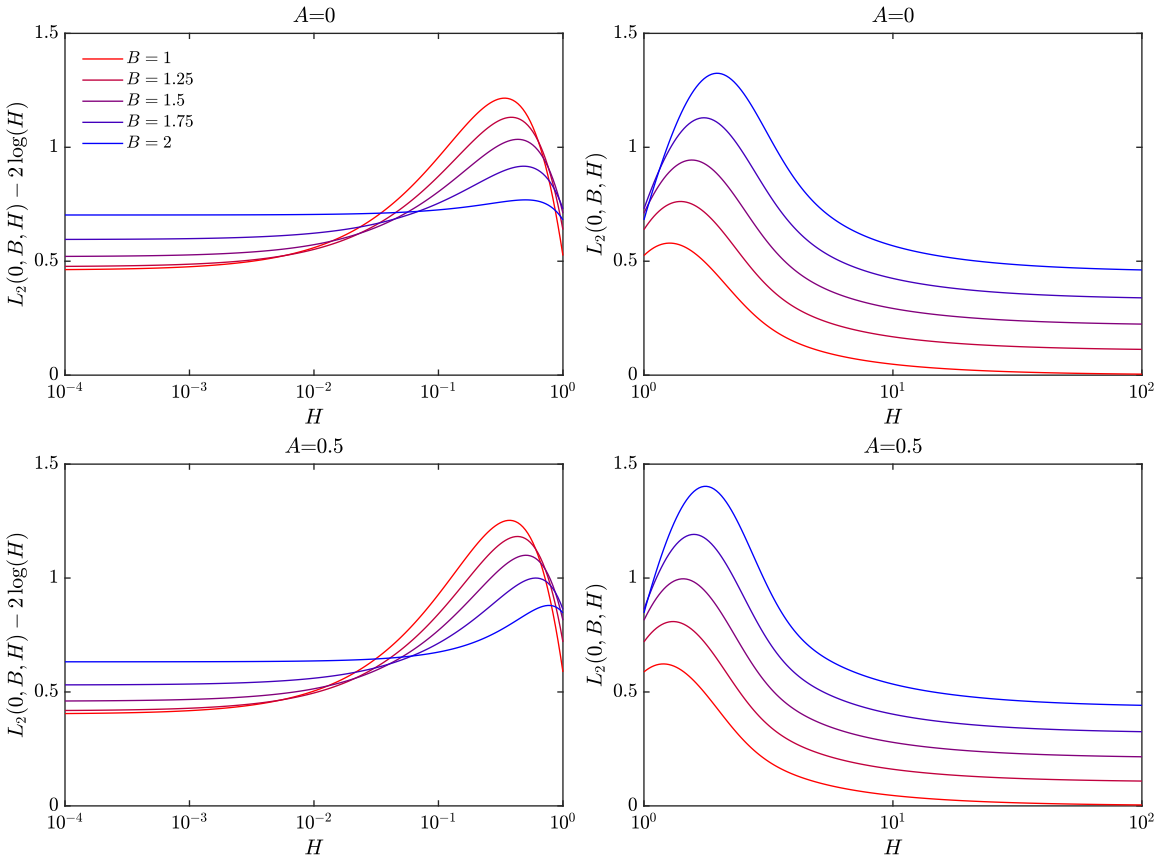

Fig. 5. The integral L_2 against H for $A = 0$ (upper plots) and $A = 0.5$ (lower plots) for various value of $1 \le B \le 2$.

$$+ \log\left(|1 - \exp\left(-\pi(A + iB_3)\right)|\right). \tag{38}$$

Since $B_3 = 2 - B_2$ we have $|1 - \exp(-\pi(A + iB_3))| = |1 - \exp(-\pi(A + iB_2))|$. Therefore G_0 exhibits the expected logarithmic singularities for $r_2 \to 0$ and $r_3 \to 0$.

There is a discontinuity between the far-field behaviour of G_0 and the far-field behaviour of G as $K \to 0$. As discussed in Section 5, the evanescent terms in the series (8) tend to zero in the far field, leaving only the propagating wave term. For, small k_0, using (36a), (37a) and (32), we have

$$G \to -\frac{\pi i}{k_0 h}\exp(ik_0 R), \quad \text{as} \quad R \to \infty,\ K \to 0. \tag{39}$$

So, in the far field, G is purely oscillatory, with the amplitude of the oscillation tending to infinity as $K \to 0$. It is easily verified that the radiation condition (1d) holds for (39). However, the radiation condition is defined for $k_0 R \to \infty$, so does not apply for zero frequency. Similarly, the limit of (39) does not exist for $R \to \infty$ and $K \to 0$ simultaneously. In contrast, from (38) we have

$$G_0 \to \frac{\pi R}{h}, \quad \text{as} \quad R \to \infty. \tag{40}$$

So, G_0 is linearly increasing with R as $R \to \infty$.

6.2. Infinite depth

Expressions for the zero-frequency GF in infinite water depth can be obtained by taking the limit of G^{deep} as $K \to 0$ or by taking the limit of G_0 as $h \to \infty$. Both results are given below. First, consider the expression for G_0 derived above and denote $C_j = \exp(-\pi(A + iB_j))$. Then we can write

$$\begin{aligned}\log(|1 - \exp(-\pi(A + iB_j))|) &= \mathrm{Re}\left(\log(1 - C_j^{1/h})\right)\\ &= \mathrm{Re}\left(\log\left(-\frac{\log(C_j)}{h} + O\left(\frac{1}{h^2}\right)\right)\right)\\ &= \log(r_j) + \log(\pi) - \log(h) + O(1/h),\end{aligned} \tag{41}$$

where the first approximation is obtained by expanding $C_j^{1/h}$ as a Laurent series and the second is obtained by expanding $\log(a+b)$ as a Taylor series. Therefore, we have

$$\lim_{h\to\infty}\left(G_0 + 2\log(h)\right) = \log(r_1) + \log(r_3) + 2\log(\pi).$$

Alternatively, starting from the infinite depth expression (31) and using (24), we have

$$\lim_{K\to 0}(G^{deep} + 2\log(K)) = \log(r_1) + \log(r_3) + 2\gamma - 2\pi i. \tag{42}$$

So both expressions have logarithmic singularities in either K or h and differ by a constant, which can be discarded in the definition of a zero-frequency GF, due to the Neumann boundary condition. We therefore define

$$G_0^{deep} \overset{\text{def}}{=} \log(r_1) + \log(r_3) \tag{43}$$

as a zero-frequency Green function for infinite depth.

7. Infinite frequency limit

In the limit $K \to \infty$ the free surface boundary condition (1b) tends to a homogeneous Dirichlet condition

$$G = 0, \quad z = 0. \tag{44}$$

As before, we consider the two cases of finite depth and infinite depth in turn below.

7.1. Finite depth

It is possible to derive limiting expressions for the integrals L_1 and L_2, by substituting limits of functions f and g from (28). However, explicit expressions can be obtained directly from the series (8). We proceed as before and note that the limits for the wavenumbers as $K \to \infty$ are

$$k_0 \to K, \tag{45a}$$

$$k_n \to (n - \tfrac{1}{2})\pi/h. \tag{45b}$$

Using these, the limits for the coefficients C_0' and C_n for $K \to \infty$ are

$$C_0' \to 1, \tag{46a}$$

$$C_n \to \frac{1}{(n-\frac{1}{2})\pi}. \tag{46b}$$

The product of the hyperbolic terms has the following limit

$$\frac{\cosh(k_0(z+h))}{\cosh(k_0 h)}\frac{\cosh(k_0(\zeta+h))}{\cosh(k_0 h)} \to \begin{cases} 1, & z=\zeta=0, \\ 0, & \text{otherwise.} \end{cases} \tag{47}$$

So the influence of the propagating wave will be zero provided that z and ζ are not both equal to zero. In the case that $z = \zeta = 0$, the limit of the propagating mode is not defined. We define the infinite frequency GF as the limit of the evanescent terms in the series

$$\begin{aligned} G_\infty \overset{\text{def}}{=} \lim_{K\to\infty}(G) &= -2\sum_{n=1}^{\infty}\frac{1}{n-\frac{1}{2}}\sin((n-\tfrac{1}{2})\pi z/h) \\ &\quad\times \sin((n-\tfrac{1}{2})\pi\zeta/h)\exp(-(n-\tfrac{1}{2})\pi A) \\ &= -\mathrm{Re}\left[\sum_{n=1}^{\infty}\frac{\exp(-(n-\frac{1}{2})\pi(A+iB_1))}{n-\frac{1}{2}}\right. \\ &\quad\left.-\sum_{n=1}^{\infty}\frac{\exp(-(n-\frac{1}{2})\pi(A+iB_3))}{n-\frac{1}{2}}\right] \\ &= -2\mathrm{Re}\left[\tanh^{-1}(\exp(-\pi(A+iB_1)/2))\right. \\ &\quad\left.-\tanh^{-1}(\exp(-\pi(A+iB_3)/2))\right] \end{aligned} \tag{48}$$

It can be verified that this expression satisfies the homogeneous Dirichlet condition on the free surface, by noticing that $B_1 = B_3$ when $z = 0$. Using the relation $B_3 = 2 - B_2$ we have $\mathrm{Re}\left[\tanh^{-1}(\exp(-\pi(A+iB_3)/2))\right] = -\mathrm{Re}\left[\tanh^{-1}(\exp(-\pi(A+iB_2)/2))\right]$. This can be used to confirm the logarithmic singularities for $r_1, r_2, r_3 \to 0$, by making use of the relation $2\tanh(x) = \log((1+x)/(1-x))$.

Provided that z and ζ are not both equal to zero, we see that, unlike the zero-frequency case, there is no discontinuity between G and G_∞ in the far field, as both tend to zero.

7.2. Infinite depth

In this case we start from the integral expression (31) and again assume that z and ζ are not both equal to zero, so that the limit of the propagating mode is zero. We have $e^{-Z}E_1(-Z) \to 0$ as $K \to \infty$ so in infinite water depth we can define

$$G_\infty^{deep} \overset{\text{def}}{=} \lim_{K\to\infty} G^{deep} = \log\left(\frac{r_1}{r_3}\right). \tag{49}$$

8. Comparison with 3D Green function

The 3D GF, denoted G_{3D}, satisfies the same free surface and sea bed boundary conditions as the 2D GF, given in Section 2. It satisfies the 3D Laplace equation and a radiation condition of the form

$$\nabla^2 G_{3D} = \frac{1}{4\pi}\delta(x-\xi)\delta(y-\eta)\delta(z-\zeta), \qquad \text{in the fluid} \tag{50a}$$

$$\frac{\partial G_{3D}}{\partial R'} = ik_0 G, \qquad R' \to \infty, \tag{50b}$$

where $R' = \left((x-\xi)^2 + (y-\eta)^2\right)^{1/2}$. To simplify the comparison, we will assume that the 3D coordinate system is aligned such that $y = \eta = 0$ and $R' = R$. In contrast to the other sections, we start by considering the infinite depth case, to illustrate the similarities between the 2D and 3D GFs.

8.1. Infinite depth

Define $M(\theta) = V_3 - iX\cos(\theta)$. Then from (31), the 2D GF for infinite depth can be written

$$G_{2D}^{deep} = \log(r_1) - \log(r_3) - 2\pi i e^{-M(0)} - 2\mathrm{Re}\left[e^{-M(0)}E_1(-M(0))\right]. \tag{51}$$

Noblesse [20] showed that the 3D infinite depth GF can be written as

$$\begin{aligned} G_{3D}^{deep} = \frac{1}{r_1} + \frac{1}{r_3} + \frac{2K}{\pi}\int_0^{\pi/2}&\left[2\pi i e^{-M(\theta)}\right. \\ &\left.+2\mathrm{Re}\left[e^{-M(\theta)}E_1(-M(\theta))\right]\right]d\theta. \end{aligned} \tag{52}$$

For the 3D GF the wave component is usually written in terms of Bessel and Struve functions using the relations (equations 9.1.18 and 12.1.7 in [47])

$$J_0(X) = \frac{2}{\pi}\int_0^{\pi/2}\cos(X\cos(\theta))d\theta, \tag{53a}$$

$$\mathbb{H}_0(X) = \frac{2}{\pi}\int_0^{\pi/2}\sin(X\cos(\theta))d\theta, \tag{53b}$$

where $\mathbb{H}_0$ and J_0 are the zero-order Struve function and Bessel function of the first kind. The 2D and 3D expressions contain the same source terms, although with a change of sign for the term involving the image of the source in the free surface. The remaining local flow and wave components for the 3D GF are given in terms of an integral over direction of the corresponding components for the 2D GF. Another key difference is that the wave and local flow components in the 3D GF are multiplied by the wavenumber, K. As discussed in Section 4, $E_1(-M)$ has a logarithmic singularity as $M \to 0$. This happens either when both the source and field point coincide on the free surface or as $K \to 0$. For the 3D case, when $K \to 0$ the GF remains finite, since the integral is multiplied by K. In contrast, in the 2D case, the logarithmic singularity is still present. In both 2D and 3D case, the logarithmic singularity is present when both source and field point coincide on the free surface.

Another important difference is the limiting behaviour of the imaginary component for $K \to 0$. In 3D, the imaginary component tends to zero, whereas in 2D the imaginary component tends to a finite limit of -2π. As the zero-frequency GF is usually defined to be purely real, for the 2D case this introduces a discontinuity between the zero-frequency GF and the limit of the 2D GF for positive frequencies. In contrast, for the 3D case, there is no discontinuity in the imaginary component. The effect of this discontinuity is discussed further in Section 9.

8.2. Finite depth

The imaginary parts of the 2D and 3D GF in finite depth can be written as [16]

$$\mathrm{Im}(G_{2D}) = -2\pi i \frac{k_0}{(k_0^2 - K^2)h + K} \frac{\cosh(k_0(z+h))}{\cosh(k_0 h)} \times \frac{\cosh(k_0(\zeta+h))}{\cosh(k_0 h)} \left[\cos(k_0 R\cos\theta)\right]_{\theta=0}, \tag{54a}$$

$$\mathrm{Im}(G_{3D}) = 2\pi i \frac{k_0^2}{(k_0^2 - K^2)h + K} \frac{\cosh(k_0(z+h))}{\cosh(k_0 h)} \times \frac{\cosh(k_0(\zeta+h))}{\cosh(k_0 h)} J_0(k_0 R), \tag{54b}$$

Using (53a) we can write

$$\mathrm{Im}(G_{3D}) = -\frac{2k_0}{\pi}\int_0^{\pi/2} \mathrm{Im}(G_{2D}(\theta))d\theta. \tag{55}$$

So the relationship between the 2D and 3D imaginary parts in finite depth is the same as that for the infinite depth case. In fact, by noting that $\mathbb{H}_0(x) = Y_0(x) + \frac{2}{\pi}O(x^{-1})$ for large x, where Y_0 is the zero-order Bessel function of the second kind, comparing the first terms in the series expansions for the 2D and 3D GFs shows that the propagating wave component of the 3D GF can be written as $-2k_0/\pi$ times the integral over direction of the propagating wave component of the 2D GF. However, there does not appear to be a general relationship between the local flow components in 2D and 3D. Instead, for the real part, we consider the integral expression and write the 2D finite depth GF as

$$\mathrm{Re}(G_{2D}) = \log(r_1) + \log(r_2) - \log(r_3) - \log(r_4) - F_1(V_3 - iX) - F_1(V_4 - iX) - L_2(A, B_1, H) - L_2(A, B_2, H) \tag{56}$$

Following a similar method to that described in [30], the real part of the 3D GF in finite depth can be written as

$$\mathrm{Re}(G_{3D}) = \frac{1}{r_1} + \frac{1}{r_2} + \frac{1}{r_3} + \frac{1}{r_4} + K\left[F_1'(V_3 - iX) + F_1'(V_4 - iX)\right] + \frac{1}{h}[L_2'(A, B_1, H) + L_2'(A, B_2, H)], \tag{57}$$

where

$$F_1'(V - iX) = \frac{2}{\pi}\int_0^{\pi/2} \left[F_1\left(V - iX\cos\theta\right)\right] d\theta \tag{58}$$

and

$$L_2'(A, B, H) = \mathrm{PV}\int_0^{\infty} \left[f(u, H)e^{-u(2+B)} + g(u, H)e^{-u(4-B)}\right] J_0(uA)du. \tag{59}$$

The 2D and 3D expressions are similar, with the deep-water components linked via the integral over angle. If we denote the integrand of L_2 as

$$N(u, A, B, H) = \left[f(u, H)e^{-u(2+B)} + g(u, H)e^{-u(4-B)}\right] \frac{\cos(uA)}{u}, \tag{60}$$

then we can write L_2 and L_2' as

$$L_2(A, B, H) = \mathrm{PV}\int_0^{\infty} N(u, A, B, H)\, du, \tag{61a}$$

$$L_2'(A, B, H) = \frac{2}{\pi}\int_0^{\pi/2} \left[\mathrm{PV}\int_0^{\infty} N(u, A\cos\theta, B, H)\, u\, du\right] d\theta. \tag{61b}$$

Table 1
Limiting real and imaginary constants in 2D and 3D Green functions for $K \to 0$.

	Re(G)		Im(G)	
	2D	3D	2D	3D
Finite depth	0	$\log(Kh)/h$	$-\pi/k_0 h$	π/h
Infinite depth	$2\log(K) + 2\gamma$	0	-2π	0

So, in contrast to the infinite depth components F_1 and F_1', the finite depth components are related by an integral over direction, but with a change of differential for the wavenumber integral from du in the 2D case to $u\,du$ in the 3D case.

In the 2D case in finite depth, the singularity in F_1 as $K \to 0$ cancels with the singularity in L_2, so that $\mathrm{Re}(G_{2D})$ remains bounded as $K \to 0$. In infinite depth, L_2 tends to a constant (see Section 4.2), so the singularity in F_1 can no longer cancel with the singularity in L_2, resulting in the singular behaviour discussed above. In the 3D case, L_2' also has a logarithmic singularity as $K \to 0$. However, as $K F_1' \to 0$ as $K \to 0$, the singularity in L_2' is not cancelled and $\mathrm{Re}(G_{3D})$ is singular for $K \to 0$ in finite depth.

A further difference between the 2D and 3D cases is the behaviour of the imaginary components. As discussed in Section 6, the imaginary component of the 2D GF is singular in the limit $K \to 0$ whereas the imaginary component of the 3D GF tends to a finite limit of π/h. A summary of the limiting real and imaginary constants in the 2D and 3D GFs for $K \to 0$ is given in Table 1.

9. Effects of low-frequency behaviour of the Green function on added mass and damping

The inconsistencies between the GF for $K \to 0$ and the GF for $K = 0$ result in inconsistencies between the added mass and damping of oscillating bodies at low frequency and zero frequency. Consider a 2D or 3D body oscillating in either the vertical (heave) or horizontal (surge) directions, with zero forward speed. To calculate the added mass and damping, we seek potentials, $\Phi_j = \mathrm{Re}\left(-i\omega\mathcal{A}\phi_j e^{-i\omega t}\right)$, $j = 1, 3$, where $j = 1$ denotes the potential for surge and $j = 3$ denotes the potential for heave and $\mathcal{A}$ is the amplitude of motion. The spatial component of the potential, ϕ_j, satisfies the same boundary conditions as the GF and additionally satisfies the body boundary condition $\partial\phi_j/\partial n = n_j$, where $n = (n_1, n_2, n_3)$ is the unit normal vector to the body surface (defined to be pointing into the body) and $n_2 = 0$ in 2D. Non-dimensional added mass and damping coefficients are defined as

$$\alpha_{ij} = \frac{1}{V}\int_S n_i \mathrm{Re}(\phi_j)dS, \tag{62a}$$

$$\beta_{ij} = \frac{1}{V}\int_S n_i \mathrm{Im}(\phi_j)dS, \tag{62b}$$

where V is the volume of the body (in the 2D case α_{ij}, β_{ij} and V are defined per unit length). Application of Green's theorem to the region bounded by the body surface, S, free surface, sea bed and a control surface located at infinity yields an integral equation for ϕ_j:

$$\Omega\phi_j + \int_S \phi_j \frac{\partial G}{\partial n}dS = \int_S n_j G dS, \tag{63}$$

where Ω is the solid angle. For a point on the body surface, Ω is equal to π in the 2D case and 2π in the 3D case. To examine the behaviour of the added mass and damping coefficients at low frequency, we subtract the limiting components of the GF that are independent of the location of the source and field points, and write

$$G = \tilde{G} + G_R + iG_I, \tag{64}$$

where G_R and G_I are the real and imaginary constants listed in Table 1. Note that by definition, $G_0 = \lim_{K\to 0}(\tilde{G})$. Also, since the constants are independent of the spatial coordinates, we have $\partial G/\partial n = \partial \tilde{G}/\partial n$. We can therefore re-write the integral equations as

$$\Omega\phi_j + \int_S \phi_j \frac{\partial \tilde{G}}{\partial n} dS = (G_R + iG_I)c_j + \int_S n_j \tilde{G} dS, \tag{65}$$

where c_j is a constant that is independent of frequency, given by

$$c_j = \int_S n_j dS = \begin{cases} 0 & j = 1, \\ S_0 - S_b & j = 3, \end{cases} \tag{66}$$

where S_0 is the water plane area and S_b is the area of the body in contact with the sea bed. We see that the constants G_R and G_I only influence the added mass and damping for vertical motions (pitch motion can also lead to a non-zero value of c_j, depending on the shape of the body and centre of rotation, but for simplicity we shall focus on heave motion here). For the case of a fully-submerged body, away from the sea bed, $c_3 = S_0 = S_b = 0$. We restrict our attention to the case of floating bodies moving in heave, for which $S_b = 0$ and $c_3 = S_0$. In the limit as $K \to 0$, the imaginary component of $\tilde{G}$ tends to zero and we can write separate equations for the real and imaginary components of the potential:

$$\Omega \mathrm{Re}(\phi_3) + \int_S \mathrm{Re}(\phi_3) \frac{\partial \tilde{G}}{\partial n} dS = G_R S_0 + \int_S n_3 \tilde{G} dS, \tag{67a}$$

$$\Omega \mathrm{Im}(\phi_3) + \int_S \mathrm{Im}(\phi_3) \frac{\partial \tilde{G}}{\partial n} dS = G_I S_0. \tag{67b}$$

As the added mass and damping are related to the real and imaginary components of the potential via (62), we see that any discontinuity between the zero frequency case and the limiting behaviour of the positive frequency case is directly related to the constants G_R and G_I. From Table 1 we can immediately infer that for a 2D floating body in infinite water depth, α_{33} tends to infinity and β_{33} tends to a finite value, whereas in deep water α_{33} tends to the zero-frequency case but β_{33} tends to infinity. Similarly, we see that for a 3D floating body in deep water, the limits of the added mass and damping are consistent with the zero-frequency case, whereas in finite depth the α_{33} tends to infinity and the β_{33} tends to a finite limit. These observation are consistent with the previous findings for 2D and 3D bodies in [41–44], discussed in the introduction.

Finally, it is worth briefly considering the low frequency behaviour of excitation forces. If we denote the diffracted potential as ϕ_d and the incident wave potential as ϕ_0, then the body boundary condition is $\partial\phi_d/\partial n = -\partial\phi_0/\partial n$. In this case $\nabla\phi_0$ is $O(k_0^2)$ as $K \to 0$, so the influence of the constants G_I and G_R also tends to zero, meaning that there is no inconsistency between the low frequency excitation forces and the zero frequency limit.

10. Discussion and conclusions

Explicit expressions for the zero-frequency and infinite-frequency GF were derived in Sections 6 and 7. In Section 3 it was noted that the series was slow to converge when R/h was close to zero. Macaskill [48] suggested subtracting the zero-frequency limit to improve the convergence of the series and avoid the need to calculate integrals. As n increases, the coefficients C_n converge quickly to the zero-frequency limit $1/n\pi$. Also, as $n \to \infty$ we have $(k_n h - n\pi) \to 0$ and $(k_n h - (n - \frac{1}{2})\pi) \to \pi/2$. So as n increases, k_n converges towards the low frequency limit and away from the high-frequency limit. The rate of convergence towards the limit depends on the value of Kh. Fig. 6 shows the difference between $k_n h$ and the low frequency limit $(k_n h \to n\pi)$ for various values of Kh. When Kh is low, the convergence towards the limit is rapid, but for higher Kh the convergence is slow. The difference between $k_n h$ and $n\pi$ results in a phase shift in the cosine terms in the series, meaning that for larger values of Kh, subtracting the low frequency limit of the series does not aid convergence. In these cases, subtracting the high frequency limit does not offer much improvement, since $k_n h$ converges away from the high frequency limit as n increases.

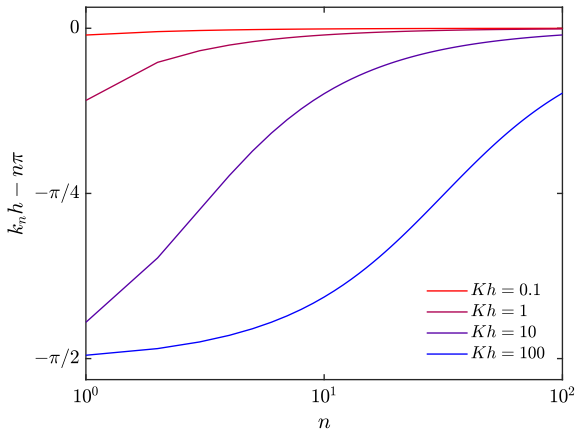

Fig. 6. Difference between nondimensional wavenumbers $k_n h$ and low frequency limit $(k_n h \to n\pi)$ for various values of Kh.

Table 2
Summary of expressions for 2D GF for various parameter ranges.

	Finite depth	Infinite depth
Near-field	$R/h \leq 0.5$, (27a)	$KR \leq 1$, (30)
Intermediate	$R/h > 0.5$, (8)	$KR > 1$, (31)
Far-field	$k_0 R \to \infty$, (32)	$KR \to \infty$, (33)
Zero-frequency	$K = 0$, (38)	$K = 0$, (43)
Infinite-frequency	$K = \infty$, (48)	$K = \infty$, (49)

It therefore appears that for low values of R/h, using the integral expressions derived in Section 4 offers a more robust method for calculating the 2D finite depth GF in the near field. The expression (27) explicitly contains the singularities when r_1, r_2 or r_3 are zero. This is advantageous for BEM models, as these components can be integrated analytically over each panel. The integrals L_1 and L_2 are convergent for all values of the parameters and are smoothly-varying, making them readily amenable for numerical approximation. Finally, the local flow component of the infinite depth GF is given explicitly, making it very fast to compute.

A summary of the expressions derived for the 2D GF for various parameter ranges is given in Table 2. An integral expression is only required for the near-field in finite depth, and a modified version of John's series [16] is used for $R/h > 0.5$ in finite depth. Explicit expressions are given for all other parameter ranges.

Declaration of competing interest

The authors declare that they have no known competing financial interests or personal relationships that could have appeared to influence the work reported in this paper.

Acknowledgement

This work was funded under EPSRC, UK grant EP/R007519/1.

References

[1] N. Salvesen, E.O. Tuck, O. Faltinsen, Ship motions and sea loads, Trans. SNAME 78 (1970) 250–287.
[2] O. Faltinsen, Sea Loads on Ships and Offshore Structures, Cambridge University Press, 1990.
[3] M. McCormick, Ocean Engineering Mechanics, Cambridge University Press, Cambridge, UK, 2010.
[4] C.M. Linton, P. Mciver, Mathematical Techniques for Wave/Structure Interactions, Chapman & Hall/CRC, 2001.
[5] C.-H. Lee, J. and Newman, Computation of wave efects using the panel method, Numerical Models in Fluid-Structure Interaction, Vol. 18, WIT Press, 2005, pp. 211–251, http://dx.doi.org/10.2495/978-1-85312-837-0/06,
[6] J.H. Milgram, Strip theory for underwater vehicles in water of finite depth, J. Eng. Math. (2007) 31–50, http://dx.doi.org/10.1007/s10665-006-9101-y.
[7] S. Sutulo, J.M. Rodrigues, C. Guedes Soares, Computation of inertial and damping characteristics of ship sections in shallow water, Ocean Eng. 36 (14) (2009) 1098–1111, http://dx.doi.org/10.1016/j.oceaneng.2009.06.013.
[8] W. Koo, J.-d. Kim, Simplified formulas of heave added mass coefficients at high frequency for various two-dimensional bodies in a finite water depth, Int. J. Naval Archit. Ocean Eng. 7 (1) (2015) 115–127, http://dx.doi.org/10.1515/ijnaoe-2015-0009.
[9] Y. Liu, H.J. Li, Iterative multi-domain BEM solution for water wave reflection by perforated caisson breakwaters, Eng. Anal. Bound. Elem. 77 (238) (2017) 70–80, http://dx.doi.org/10.1016/j.enganabound.2016.12.011.
[10] K.G. Vijay, S. Neelamani, T. Sahoo, Wave interaction with multiple slotted barriers inside harbour: Physical and numerical modelling, Ocean Eng. 193 (2019) 106623, http://dx.doi.org/10.1016/j.oceaneng.2019.106623.
[11] E. Mackay, L. Johanning, Comparison of analytical and numerical solutions for wave interaction with a vertical porous barrier, Ocean Eng. 199 (2020) 107032, http://dx.doi.org/10.1016/j.oceaneng.2020.107032.
[12] B. Molin, Hydrodynamic modeling of perforated structures, Appl. Ocean Res. 33 (1) (2011) 1–11.
[13] S. An, O.M. Faltinsen, An experimental and numerical study of heave added mass and damping of horizontally submerged and perforated rectangular plates, J. Fluids Struct. 39 (2013) 87–101, http://dx.doi.org/10.1016/j.jfluidstructs.2013.03.004.
[14] J.S. Dokken, J. Grue, L.P. Karstensen, Wave forces on porous geometries with linear and quadratic pressure-velocity relations, in: 32nd International Workshop on Water Waves and Floating Bodies, Dalian, China, 2017.
[15] T. Havelock, The damping of the heaving and pitching motion of a ship, The London, Edinburgh, and Dublin Phil. Mag. J. Sci. 33 (224) (1942) 666–673.
[16] F. John, On the motion of floating bodies II. Simple harmonic motion, Comm. Pure Appl. Math. 3 (1950) 45–101, http://dx.doi.org/10.1002/cpa.3160030106.
[17] M. Haskind, On wave motion of a heavy fluid, Prikl. Mat. Mekh. 18 (1954) 15–26.
[18] T. Havelock, Waves due to a floating sphere making periodic heaving oscillations, Proc. Roy. Soc. A 231 (1955) 1–7.
[19] W. Kim, On the harmonic oscillations of a rigid body on a free surface, J. Fluid Mech. 21 (1965) 427–451.
[20] F. Noblesse, The green function in the theory of radiation and diffraction of regular water waves by a body, J. Eng. Math. 16 (1982) 137–169.
[21] J.N. Newman, An expansion of the oscillatory source potential, Appl. Ocean Res. 6 (2) (1984) 116–117, http://dx.doi.org/10.1016/0141-1187(84)90049-X.
[22] J.N. Newman, Algorithms for the free-surface green function, J. Eng. Math. 19 (1) (1985) 57–67, http://dx.doi.org/10.1007/BF00055041.
[23] J. Telste, F. Noblesse, Numerical evaluation of the green function of water wave radiation and diffraction, J. Ship Res. 30 (2) (1986) 69–84.
[24] B. Ponizy, F. Noblesse, M. Ba, M. Guilbaud, Numerical evaluation of free-surface green functions, J. Ship Res. 38 (3) (1994) 193–202.
[25] C. Linton, Rapidly convergent representations for green 's functions for Laplace 's equation, Proc. R. Soc. Lond. Ser. A Math. Phys. Eng. Sci. 455 (1999) 1767–1797, http://dx.doi.org/10.1098/rspa.1999.0379.
[26] Y. Liu, H. Iwashita, C. Hu, A calculation method for finite depth free-surface green function, Int. J. Naval Arc. Ocean Eng. 7 (2) (2015) 375–389, http://dx.doi.org/10.1515/ijnaoe-2015-0026.
[27] C. Xie, Y. Choi, F. Rongère, A.H. Clément, G. Delhommeau, A. Babarit, Comparison of existing methods for the calculation of the infinite water depth free-surface Green function for the wave – structure interaction problem, Appl. Ocean Res. 81 (2018) 150–163.
[28] J.N. Newman, The approximation of free-surface green functions, in: G.R. Martin (Ed.), Wave Asymptotics, Cambridge University Press, 1992, pp. 107–135.
[29] X. Chen, Evaluation de la fonction de Green du probleme de diffraction/radiation en profondeur d'eau finie-une nouvelle methode rapide et precise, in: Actes des 4e Journees de l'Hydrodynamique, Nantes, France, 1993, pp. 371–384.
[30] E. Mackay, Consistent expressions for the free-surface green function in finite water depth, Appl. Ocean Res. 93 (2019) 101965, http://dx.doi.org/10.1016/j.apor.2019.101965.
[31] M.A. Peter, M.H. Meylan, The eigenfunction expansion of the infinite depth free surface green function in three dimensions, Wave Motion 40 (1) (2004) 1–11, http://dx.doi.org/10.1016/j.wavemoti.2003.10.004.
[32] A.H. Clément, A second order Ordinary Differential Equation for the frequency domain Green function, in: Proceedings 28th international workshop on water waves and floating bodies, Marseille, France, 2013.
[33] Y. Shen, D. Yu, W. Duan, H. Ling, Ordinary differential equation algorithms for a frequency-domain water wave green's function, J. Eng. Math. 100 (1) (2016) 53–66, http://dx.doi.org/10.1007/s10665-015-9833-7.
[34] C. Xie, X. Chen, A.H. Clément, A. Babarit, A new ordinary differential equation for the evaluation of the frequency- domain Green function, Appl. Ocean Res. 86 (2019) 239–245, http://dx.doi.org/10.1016/j.apor.2019.03.003.
[35] H. Wu, C. Zhang, Y. Zhu, W. Li, D. Wan, F. Noblesse, A global approximation to the green function for diffraction radiation of water waves, Eur. J. Mech. B/Fluids 65 (2017) 54–64, http://dx.doi.org/10.1016/j.euromechflu.2017.02.008.
[36] R. Thorne, Multipole expansions in the theory of surface waves, Math. Proc. Cambridge Philos. Soc. 49 (4) (1953) 707–716.
[37] J.V. Wehausen, E. Laitone, Surface waves, Encycl. Phys. i (1960) 446–778.
[38] C.C. Mei, The Applied Dynamics of Ocean Surface Waves, World Scientific, 1983.
[39] R. Hein, M. Durán, J.-C. Nédélec, Explicit representation for the infinite-depth two-dimensional free-surface Green's function in linear water-wave theory, SIAM J. Appl. Math. 70 (7) (2010) 2353–2372.
[40] F. Noblesse, Analytical representation of ship waves, Ship Technol. Res. 48 (2001) 23–48.
[41] X. Chen, C. Ouled Housseine, C. Xie, New analysis on the green function in water of finite depth, in: 30th International Offshore and Polar Engineering Conference, 2020, pp. 1758–1764.
[42] F. Ursell, On the virtual-mass and damping coefficients for long waves in water of finite depth, J. Fluid Mech. 76 (1) (1976) 17–28, http://dx.doi.org/10.1017/S0022112076003091.
[43] P. McIver, C.M. Linton, The added mass of bodies heaving at low frequency in water of finite depth, Appl. Ocean Res. 13 (1) (1991) 12–17, http://dx.doi.org/10.1016/S0141-1187(05)80036-7.
[44] J. Kotik, V. Mangulis, On the kramers-kronig relations for ship motions, Int. Shipbuild. Prog. 9 (1962) 361–368, http://dx.doi.org/10.3233/ISP-1962-99701.
[45] L.F. Shampine, Vectorized adaptive quadrature in MATLAB, J. Comput. Appl. Math. 211 (2) (2008) 131–140, http://dx.doi.org/10.1016/j.cam.2006.11.021.
[46] I.S. Gradshteyn, I.M. Ryzhik, Table of Integrals, Series, and Products, 7th Edition, Academic Press, 2007.
[47] M. Abramowitz, I. Stegun, HandBook of Mathematical Functions, United States Department of Commerce, National Bureau of Standards, 1964.
[48] C. Macaskill, Reflexion of water waves by a permeable barrier, J. Fluid Mech. 95 (1) (1979) 141–157, http://dx.doi.org/10.1017/S0022112079001385.